IEEE Access
Multidisciplinary ⋮ Rapid Review ⋮ Open Access Journal

Received 8 October 2025, accepted 28 October 2025, date of publication 30 October 2025, date of current version 5 November 2025.

Digital Object Identifier 10.1109/ACCESS.2025.3627384

TOPICAL REVIEW

Grid-Connected Power Converters for Electrolysis Applications

MOHAMMADHOSSEIN TAVANAEE, (Graduate Student Member, IEEE),
JAUME GIRONA-BADIA, (Member, IEEE),
MARC CHEAH-MAÑE, (Senior Member, IEEE),
ORIOL GOMIS-BELLMUNT, (Fellow, IEEE),
AND EDUARDO PRIETO-ARAUJO, (Senior Member, IEEE)
CITCEA-UPC, Department of Electrical Engineering, Universitat Politècnica de Catalunya, 08028 Barcelona, Spain

Corresponding author: Mohammadhossein Tavanaee (mohammadhossein.tavanaee@upc.edu)

This work was supported by the European Union's Horizon Europe Programme within the H2GLASS Project, under Grant 101092153. The work of Oriol Gomis-Bellmunt was supported by the ICREA Academia Programme.

ABSTRACT The growing demand for efficient and sustainable hydrogen production highlights the need for converter topologies that comply with grid code requirements and contribute toward the stability of the power system in electrolysis applications. In this paper, several converter topologies are reviewed and analyzed based on the performance of the most common electrolyzers, PEM and AEL. Traditional diode and thyristor-based rectifiers are explored, emphasizing their reliability and robustness while highlighting their flexibility limitations. IGBT-based power converters are also introduced, demonstrating their potential for electrolysis applications with faster response times and improved power quality. A comprehensive comparative analysis under steady-state and fault conditions is presented, offering critical insights into the converter choices for future large-scale hydrogen production.

INDEX TERMS Hydrogen production, electrolyzer types, converter topologies, dynamic analysis.

I. INTRODUCTION

The demand for hydrogen is anticipated to grow by a factor of more than 10 in 2050 due to the worldwide goal of achieving net zero carbon emissions and the shift to using hydrogen-based e-fuels rather than fossil fuels [1]. Nevertheless, the majority of the world's hydrogen generation relies on the steam reforming of natural gas, which results in annual CO_2 emissions of around one million tonnes [2]. On the other hand, water electrolysis is a specific way of producing hydrogen and is the source of 4% of worldwide hydrogen production [3], in which water is split into hydrogen and oxygen using electric power. Therefore, the methods used to generate electricity greatly influence how much CO_2 is released when hydrogen is produced by water electrolysis. Using electricity generated by fossil fuels will result in considerable carbon emissions. However, the energy generated by renewable energy sources like wind and photovoltaics has low carbon emissions. For the mentioned reason, hydrogen produced using electricity derived from non-renewable sources is called gray hydrogen, whereas the hydrogen produced using renewable sources is referred to as green hydrogen [4].

There are several types of electrolyzers available depending on how they move ions and electrolytes, but alkaline (AEL) and proton exchange membrane (PEM) electrolyzers are the most common [5]. Despite being more expensive, PEM electrolyzers are more efficient and last longer. Nevertheless, the AEL electrolyzers are more mature technology, less expensive, and have a higher hydrogen production rate, but they are more corrosive, and the electrodes have a shorter lifespan [6].

Industrial-size AEL and PEM electrolyzers must be connected to a DC power supply, which has DC voltage

The associate editor coordinating the review of this manuscript and approving it for publication was Santu Giri.

(a few hundred volts) and direct current (up to thousands of amps). Common topologies for this purpose are diode-based and thyristor-based rectifiers. The DC voltage quality and the high harmonic distortion generation are the main issues with the aforementioned topologies, particularly in thyristor-based rectifiers. It is unavoidable to mitigate them with large filters, but they are reliable and economical.

This review presents an overview of AEL and PEM electrolyzers, detailing their operational characteristics and advancements. In addition to traditional diode and thyristor rectifiers, it also covers more recent power conversion technologies such as voltage source converters (VSCs) in both single and two-stage configurations. By examining these technologies, the review aims to offer a comprehensive comparison of the different converter technologies used in electrolysis applications, emphasizing their performance under steady-state conditions as well as during fault events. To the best of the author's knowledge, there is a lack of comprehensive studies that provide a comparative analysis of these technologies for electrolysis applications addressing both normal operation and fault conditions.

The structure of the paper is as follows: AEL and PEM are explained in Section II. Section III evaluates uncontrolled rectifiers that use diode switches. Section IV presents controlled rectifiers based on thyristor valves. Forced-commuted rectifiers are examined in Section V, along with their benefits over other technologies. Two-stage converters are presented in Section VI. The comparison of power converters is detailed in Section VII, and the conclusion is provided in Section VIII.

II. ELECTROLYSER TYPES

Electrolyzers are offered in a variety of sizes, from little appliances that are ideal for small-scale dispersed hydrogen generation to massive central production plants that might be connected directly to non-greenhouse gas-generating sources of energy [7]. The following overview of AEL and PEM electrolyzers provides essential background for the discussions that follow.

A. ALKALINE ELECTROLYZER

The AEL electrolyzer is one of the most mature and widely used electrolyzers on the market. It employs two electrodes submerged in an electrolyte solution of potassium hydroxide (KOH) or sodium hydroxide (NaOH), typically at a concentration of 20–40% of weight. Due to the former electrolyte solution's superior conductivity (average specific conductivity of a 27% of weight KOH solution is around 0.65 S/cm (at 25 °C), KOH is favored over NaOH [8]. A diaphragm membrane separates the two electrodes and allows the hydroxide ions (OH^-) to move from the cathode to the anode [9], [10]. The chemical reaction equations [11], can be written as

$$4OH^- \rightarrow O_2 + 2H_2O + 4e^- \quad \text{(Anode)} \tag{1a}$$

$$2H_2O + 2e^- \rightarrow H_2 + 2OH^- \quad \text{(Cathode)} \tag{1b}$$

$$2H_2O \rightarrow 2H_2 + 2O_2 \quad \text{(Overall)} \tag{1c}$$

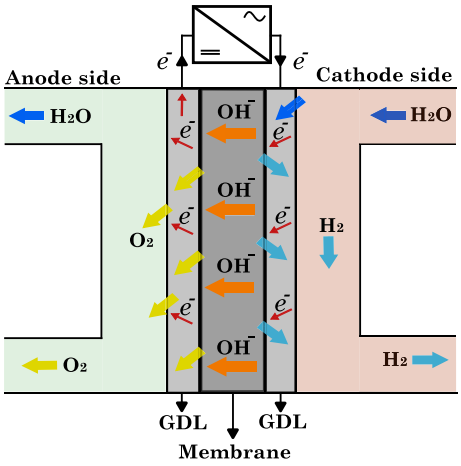

FIGURE 1. Alkaline electrolyzer.

AEL water electrolysis cells come in two main varieties: (i) gap cells, where the electrodes are separated from the cell separator, and (ii) zero-gap cells, where porous electrodes are in direct contact with the separator. In gap cells, gas screening effects during gas generation at higher current densities limit the maximum operational current density to a few hundred mA/cm^2. By contrast, zero-gap cells, introduced in 1967 [12], minimize this limitation due to their compact design, although their operational current density is still influenced by factors such as electrode and membrane properties.

A zero-gap design facilitates the transfer of gases and liquids to and from the electrodes using separators such as screens, grids, or porous electrodes [13]. Maintaining an optimal electrolyte concentration requires a continuous water supply, as water is the sole reactant in the electrochemical process. At typical operating temperatures ($60 - 80°C$), gas products also carry away water vapor and residual electrolytes.

The cathode side is supplied with pure water, as shown in Fig. 1. At the cathode side, the water and electrons react to produce hydrogen (H_2) and hydroxide ions (OH^-). Then, electrons move to the anode side via the gas diffusion layer (GDL), and hydroxide ions are transferred to the anode side by the liquid electrolyte while the (O) is generated at the anode side.

To analyze the electric interconnection of the electrolyzer, an electrical equivalent model is typically used. There have been several studies on modeling the AEL electrolyzer and its coupling with renewable energy sources; however, in [14], electrical modeling is divided into static and dynamic models. As depicted in Fig. 2, the following are the components of the dynamic model:

- V_{rev} represents the reversible voltage, which is the minimum voltage required to split water into hydrogen and oxygen under standard conditions and is modeled as a DC voltage source.
- i_{act} is a current source in parallel with a capacitor C_a and both together represent activation overvoltage and, in particular, the double-layer [15] phenomenon

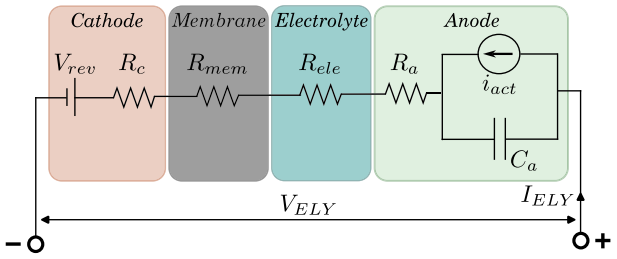

FIGURE 2. Alkaline electrolyzer electrical dynamic equivalent.

between an electrode (anode or cathode) and an electrolyte.

- R_a, R_c, R_{mem}, and R_{ele} comprise respectively the anode, cathode, membrane, and electrolyte losses.

B. PEM ELECTROLYZER

To address the limitations of AEL electrolyzers, a solid sulfonated polystyrene membrane was proposed as the electrolyte [16], [17]. PEM, or polymer electrolyte membrane water electrolysis, is another name for this concept. The solid polymer electrolyte (SPE) used in PEM electrolyzers serves as both a reactant barrier to prevent gas crossing, while also exchanging protons from the anode to the cathode and separating the produced gases from the anode and cathode. The following summarizes the chemical processes involved in PEM water electrolysis [18]

$$2H_2O \rightarrow O_2 + 4H^+ + 4e^- \text{ (Anode)} \quad (2a)$$

$$4H^+ + 4e^- \rightarrow 2H_2 \quad \text{(Cathode)} \quad (2b)$$

$$2H_2O \rightarrow 2H_2 + O_2 \quad \text{(Overall)} \quad (2c)$$

In PEM water electrolysis, hydrogen and oxygen are electrochemically separated from water at their respective electrodes. Pumping water to the anode, where it is divided into oxygen (O_2), protons (H^+), and electrons (e^-), yields PEM water electrolysis. The particle membrane allows these protons to move from the anode side to the cathode side. The external power circuit, which supplies the reaction's driving force (cell voltage), allows the electrons to leave the anode. At the cathode side, protons and electrons recombine to form hydrogen, as depicted in Fig. 3 [19].

On one hand, PEM electrolyzers have higher output densities and efficiency gains than AEL technology, satisfactory partial load ranges, smaller stack designs, high-pressure operation, and quicker dynamic reaction times. On the other hand, using noble materials such as iridium and platinum may lead to higher costs [20]. Currently, perfluorosulfonic acid polymers like Nafion, Felmion, Fumapem, or Aciplex are often used to make electrolytes. These polymers have excellent conductivity for proton transport, good mechanical strength, and great oxidative stability. The proton conductivity is >0.1 Scm^{-2} at membrane thicknesses of 100 μm to 200 μm, which reduces resistive loss and enables operation at greater operating current densities, and therefore these polymers are used for low-cost AEL electrolyzers [21].

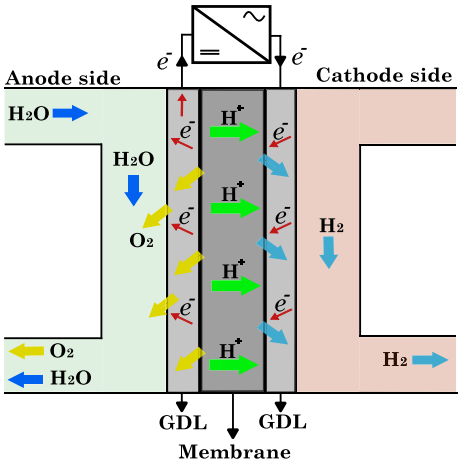

FIGURE 3. PEM electrolyzer.

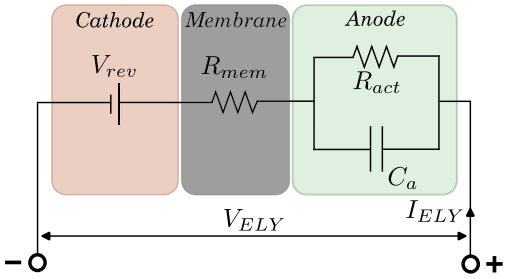

FIGURE 4. PEM electrolyzer electrical dynamic equivalent.

Similar to the electrical analysis of AEL electrolyzers, there is interest in the scientific community in modeling the PEM electrolyzer from an electrical point of view. In [22], both static and dynamic models are created and compared to actual results from a real PEM electrolyzer, and it is concluded that the dynamic model has a maximum error of about 4%, while the static model has a maximum error of about 15% (especially noticeable in the electrical current step changes), implying that the dynamic model has higher accuracy than the static model. The dynamic model presented in [23] includes an open-circuit voltage, or reversible voltage (V_{rev}) at $i_{el} = 0$, which is dependent on the electrolyzer parameters. Overpassing the V_{rev} causes a jump in current value, which indicates that the electrolyzer has begun to operate. The rise in current can be modeled as ohmic losses in the membrane, and the voltage-current (VI) variation, as shown in [24], indicates a first-order response, which can be modeled as an RC parallel branch in the anode and cathode. Also, it was recognized and mentioned in [22] that because the anode's chemical reactions occur more quickly than those of the cathode, more dynamics are concentrated there, allowing the cathode dynamics to be disregarded. Fig. 4 shows the PEM electrolyzer's electrical equivalent model.

In Table 1, an overview comparison of PEM and AEL electrolyzers is provided. After the entirety of what has been stated about PEM and AEL electrolyzers, one essential requirement is the necessity of direct current for electrolysis

TABLE 1. Comparison of PEM and AEL electrolyzers [21], [25].

Aspect	PEM	AEL
Dynamics	Fast (s-min)	Moderate (min-hrs)
Operating T(°C)	50-80 °C	60-90 °C
Degradation rate	Low	High
Efficiency	(70-80%)	(60-70%)
Lifespan	10.000 hrs	10.000-100.000 hrs

applications. As a consequence, several rectifiers that may be suited for this use are analyzed in the following sections.

III. UNCONTROLLED RECTIFIERS

Uncontrolled rectifiers are a particular kind of AC/DC converter that generates a set DC output voltage from a predetermined AC input source. Uncontrolled rectifiers, as the name implies, are unable to regulate the magnitude of the rectified DC voltage, and the rectification process is normally carried out using uncontrolled switching devices like diodes. In order to adjust the DC voltage, it is required to vary the AC voltage, which can be done by employing autotransformers [26]. Some uncontrolled rectifiers for electrolysis applications are listed below.

A. THREE-PHASE BRIDGE RECTIFIERS

Three-phase bridge rectifiers are commonly employed in high-power applications due to their efficient utilization of transformers and lower ripple factors compared to single-phase rectifiers. The reduced ripple factor leads to a smoother DC output voltage, making the rectifier more cost-effective by minimizing the need for extensive filtering components. The average DC output voltage V_{dc} and the RMS voltage V_{RMS} of a three-phase bridge rectifier are given by [27]:

$$V_{\text{dc}} = \frac{3\sqrt{3}}{\pi} V_{\text{m}} = 1.654\ V_{\text{m}} \tag{3}$$

$$V_{\text{ELY,(RMS)}} = V_{\text{m}} \sqrt{\frac{3}{2} + \frac{9\sqrt{3}}{4\pi}} = 1.655\ V_{\text{m}} \tag{4}$$

where V_{m} is the peak phase voltage of the AC supply. The DC voltage represents the steady component of the rectified output, which determines the effective power supplied to a DC load. In contrast, the RMS voltage accounts for the equivalent heating effect of the varying rectified waveform, which is essential for analyzing losses and ripple in the system.

The ripple factor γ for the three-phase bridge rectifier is significantly lower than that of single-phase rectifiers and is calculated as:

$$\gamma = \sqrt{(\frac{V_{\text{RMS}}}{V_{\text{dc}}})^2 - 1} = 0.042 \tag{5}$$

This low ripple factor indicates that the output voltage is close to pure DC, reducing the necessity for extensive filtering. The operation of the three-phase bridge rectifier involves six diodes arranged in a bridge configuration. During each $\pi/3$ interval of the AC cycle, two diodes conduct, one from the upper group and one from the lower group, allowing current to flow through the load in the same direction. This sequential conduction results in a more constant DC output voltage [28].

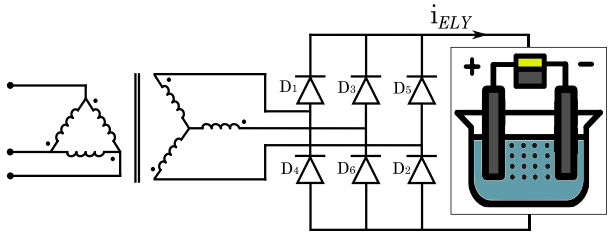

FIGURE 5. Three-phase bridge rectifier.

B. THREE-PHASE DOUBLE-STAR RECTIFIER WITH INTER-PHASE TRANSFORMER

High reverse voltage can stress the diodes, potentially leading to breakdown, increased power losses, and reduced reliability of the rectifier [29]. One way to reduce the level of reverse voltage in the diodes is to modify the previous configuration to the one shown in Fig. 6. This configuration comprises two three-phase star rectifiers with their neutral points coupled by an inter-phase transformer (IPT) or reactor. The IPT operates by facilitating the flow of circulating currents between the rectifier bridges, thereby compensating for voltage imbalances and ensuring equitable current distribution. The polarities of the transformer's secondary side are opposite between them, so while one is at its maximum, the other is at its lowest. Since the frequency of the output voltage is six times that of the input AC voltage, the DC filter is reduced. In comparison to the star topology, this design provides reduced RMS current for the diodes and a higher energy efficiency. The output DC voltage can be calculated as

$$V_{\text{dc}} = \sqrt{3}\alpha V_{\text{ph}} \tag{6}$$

where α is the transformer turn ratio, and V_{ph} is the input phase to ground voltage.

C. SIX-PHASE STAR RECTIFIERS

Fig. 7 displays the six-phase star rectifier, also known as the three-phase full-wave rectifier. In this topology, the output DC voltage ripple is lowered compared to the simple star configuration, and each diode conducts $\pi/3$ instead of $2\pi/3$, resulting in low average current and improved efficiency [30]. The output voltage's DC and RMS values are as follows:

$$V_{\text{dc}} = V_{\text{m}} \frac{6}{\pi} \frac{1}{2} = 0.955\ V_{\text{m}} \tag{7}$$

$$V_{\text{ELY,(RMS)}} = V_{\text{m}} \sqrt{\frac{6}{2\pi} \left(\frac{\pi}{6} + \frac{\sqrt{3}}{4} \right)} = 0.956\ V_{\text{m}} \tag{8}$$

D. TWELVE-PULSE SERIES BRIDGE RECTIFIER

The twelve-pulse series bridge rectifier is typically utilized when a greater voltage is needed. The output voltage of

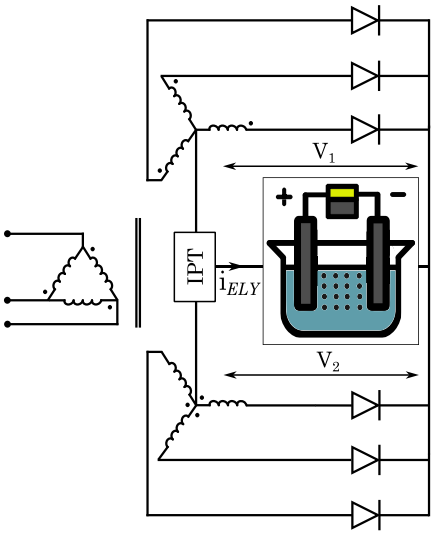

FIGURE 6. Three-phase double-star rectifier with inter-phase transformer.

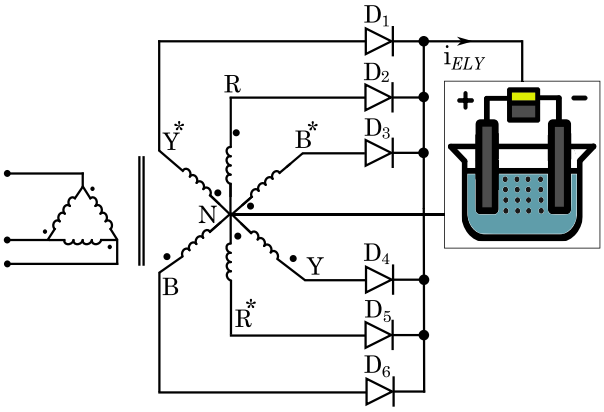

FIGURE 7. Six-phase star rectifier.

the transformer will naturally phase shifted by $\pi/6$ when employing the star-delta configuration on the secondary side. As can be seen in the Fig. 8, by connecting star and delta windings in series, the output ripple frequency is made to be 12 times that of the input frequency, resulting in less output voltage ripple than the other rectifier topologies. The output voltages can be written as [27]

$$V_{\mathrm{dc}} = V_{\mathrm{m}} \frac{12}{\pi} \frac{\sqrt{3}-1}{2\sqrt{2}} = 0.98862\ V_{\mathrm{m}} \tag{9}$$

$$V_{\mathrm{ELY,(RMS)}} = V_{\mathrm{m}} \sqrt{\frac{12}{2\pi}\left(\frac{\pi}{12} + \frac{1}{4}\right)} = 0.98867\ V_{\mathrm{m}} \tag{10}$$

E. TWELVE-PULSE PARALLEL BRIDGE RECTIFIER (WITH INTER-PHASE TRANSFORMER)

In comparison to the twelve-pulse series rectifier, the 12-pulse parallel bridge rectifier is often utilized for greater currents because it distributes the total current load between

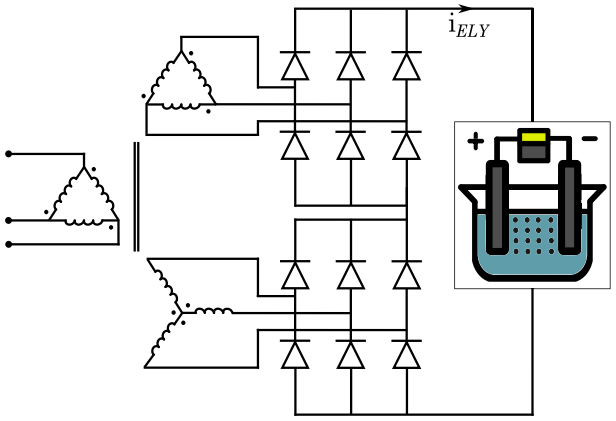

FIGURE 8. 12-pulse series bridge rectifier.

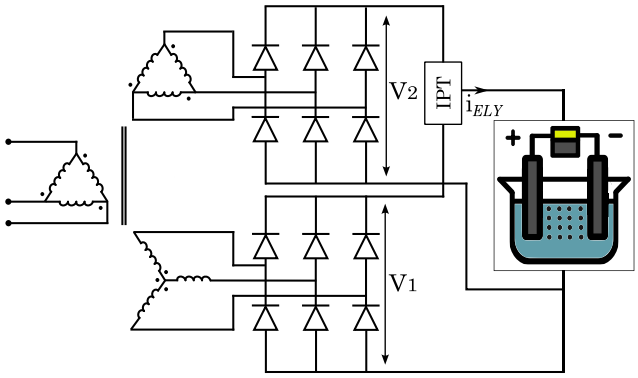

FIGURE 9. 12-pulse parallel bridge rectifier (with inter-phase transformer).

TABLE 2. Comparison of uncontrolled rectifiers.

Indices	3ph Bridge	Double star with IPT	6ph Star	12-pulse Series	12-pulse Parallel with IPT
Diode Reverse Voltage	1.05 Vdc	1.06 Vdc	2.09 Vdc	0.524 Vdc	1.05 Vdc
Diode RMS Current	0.579 Idc	0.293 Idc	0.409 Idc	0.596 Idc	0.409 Idc
Ripple Factor	0.042	0.042	0.042	0.01	0.01
Rectification Ratio	0.998	0.998	0.998	1	1

two parallel rectifier bridges. The output voltage is expected to be the average of the rectified voltages V_1 and V_2 (Fig. 9) due to the inter-phase transformer's existence. The output frequency will be multiplied by 12, similar to the 12-pulse series rectifier; the voltage ripple is small (approximately 1%), and the voltage values are the same as (9) and (10) [27]. The benefits of this topology include a good power factor and minimal harmonic content, while the system's complexity and costs arise from the need for precise phase shifting, synchronization, and the additional components required, such as the inter-phase transformer. In summary, a brief comparison of uncontrolled rectifiers for design purposes is presented in Table 2.

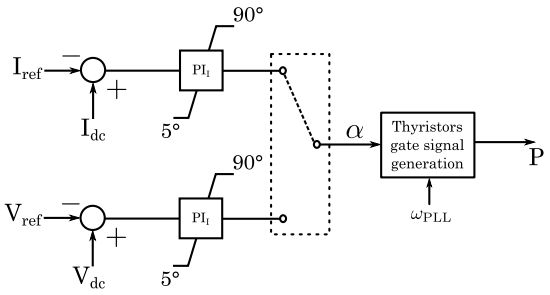

FIGURE 10. Control structure for thyristor-based converters.

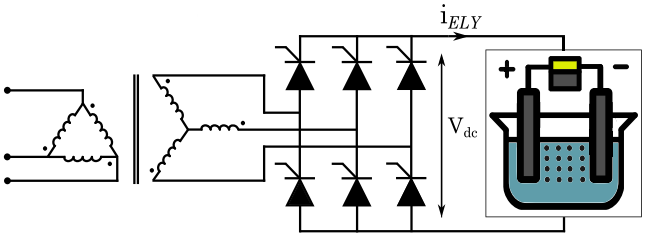

FIGURE 11. Three-phase full-wave thyristor-based rectifier.

IV. CONTROLLED RECTIFIERS

The second class of rectifiers, known as controlled rectifiers, employ thyristors instead of diodes, allowing for the regulation of current through the electrolyzer and hydrogen generation. This control flexibility is particularly beneficial when the electrolyzer is connected to renewable energy sources [5]. Thyristor-based rectifiers currently rule the industrial market for applications where high power is needed to operate electrolyzers [31], [32], [33]. The firing angle (α) is used to describe the angle at which a thyristor is set to conduct throughout each half-cycle of an alternating current and is the key to controlling thyristors. When the firing angle is less than $\pi/2$ the rectifier is in rectifier mode; in contrast, when the firing angle is between $\pi/2$ and π, the rectifier operates in inverter mode [34]. Fig. 10

depicts a basic control structure for thyristor-based converters, whereby various firing angles may be created based on reference current or voltage, the complete control design is explained in [35].

It is worth mentioning that varying the firing angle increases the current harmonic content injected into the AC network, which reduces the power factor, so additional filters must be introduced to reduce harmonics [36]. Different types of controlled thyristor-based rectifiers are presented in this section.

A. THREE-PHASE FULL-WAVE THYRISTOR-BASED RECTIFIER

The three-phase full-wave rectifier, also known as a Graetz bridge, is depicted in Fig. 11; as can be seen, thyristors are used in place of diodes. By assuming ideal conditions, the average DC voltage of this rectifier is [27]

$$V_{dc} = \frac{3V_{max}\sqrt{3}}{\pi}\cos\alpha = 1.65\ V_{max}\cos\alpha \qquad (11)$$

The DC voltage is highly dependent on firing angle α according to (11), raising the firing angle reduces the output voltage, but the firing angle should not exceed $\pi/2$ in order to retain the rectifier mode. The benefits of this system are reasonable efficiency and high power handling capacity, and the disadvantages are large current ripple at the DC side and poor power quality at the AC side, specifically reactive power that is inversely proportional to the firing angle. To reduce the output voltage under partial load, the firing angle must be increased, which leads to a low power factor, significant losses, and DC-current ripple. However, a greater current ripple increases the PEM electrolyzer's specific energy consumption, meaning that the electrolyzer requires more energy per unit of hydrogen produced. This occurs because fluctuations in the current lead to inefficient electrochemical reactions, resulting in lower hydrogen production efficiency and increased heat dissipation [37]. Moreover, the system will require a large-scale active or passive filtering solution, raising the overall cost [38].

B. DOUBLE-STAR RECTIFIER WITH INTER-PHASE TRANSFORMER

A double-star rectifier with an inter-phase transformer introduces fewer harmonics into the system compared to the previous topology and is typically used in high-power applications. The two thyristor-based rectifiers are moved by 180°, and the negative pole of the electrolyzer is linked to the neutral nodes of the secondary transformer through an inter-phase transformer [27], as illustrated in Fig. 12. The positive aspect of employing this double-star rectifier as opposed to a three-phase full-wave rectifier is the reduction in output current ripple as well as the thyristor average and RMS current (which is 50% lower). As a result, the specific energy consumption is decreased and the hydrogen production quality is improved [5].

C. 12-PULSE THYRISTOR-BASED BRIDGE RECTIFIER

The 12-pulse thyristor-based bridge rectifier (See Fig. 13), which is typically used in high-current applications including electrolysis, consists of two bridge thyristor-based rectifiers coupled in parallel. But so far, it may be used in high-voltage applications by connecting them in series. This arrangement provides better power quality and lower current ripple compared to the Graetz rectifier [5]. However, it is important to note that the main drawback of thyristor-based rectifiers is the need for reactive power compensation as a result of harmonic production. For instance, employing Flexible AC Transmission System (FACTS) devices for this topology's reactive power correction might result in a power factor of 0.98, as mentioned in [39].

V. FORCED-COMMUTATED CONTROLLED RECTIFIERS

In forced-commutated converters, semiconductors with gate-turn-off capabilities (e.g., IGBTs, MOSFETs) are used

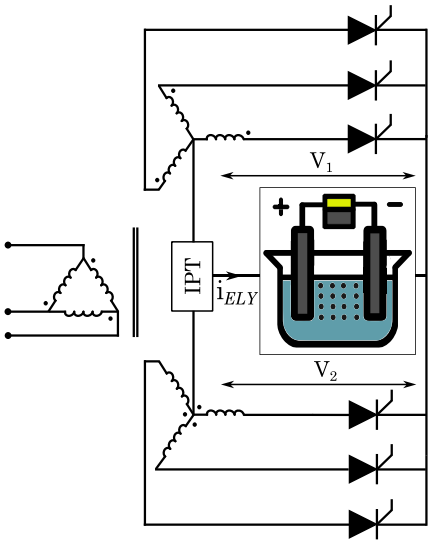

FIGURE 12. Six-pulse double-star thyristor-based rectifier with inter-phase transformer.

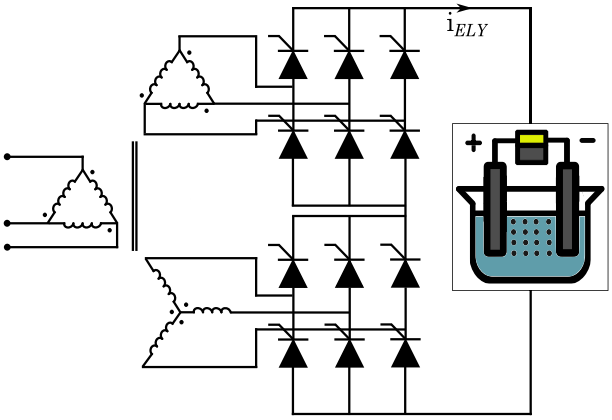

FIGURE 13. 12-pulse thyristor-based rectifier.

for enhanced controllability, allowing frequent switching between ON and OFF states. Unlike thyristor-based line-commutated rectifiers, which remain open until the end of the period after a firing pulse, these semiconductors can switch hundreds of times within a single period. Such capability might offer benefits including reduced harmonic production, the capability of adjusting power factor, and the ability to build voltage or current source converters [27]. Leveraging forced-commutated rectifiers for large power electrolyzers where large currents with low voltage are required can be challenging, but thanks to recent advances in control and in the production of power electronic components, they are the potential alternative to diode and thyristor-based rectifiers.

A. VOLTAGE SOURCE CONVERTER

VSCs are a type of forced-commutated rectifiers that are widely used in applications where control of active and reactive power is required. A VSC is capable of converting DC voltage into AC voltage at a controlled magnitude and

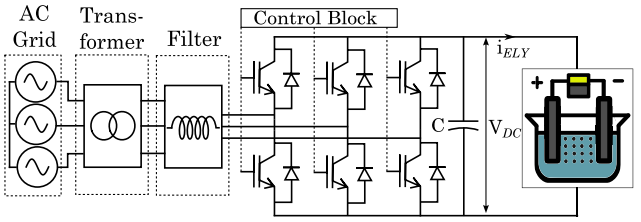

FIGURE 14. Voltage source converter.

frequency, or vice versa, and can facilitate bidirectional power flow [40]. The flexibility of VSCs lies in their ability to generate any waveform using pulse-width modulation (PWM) or other switching strategies, allowing for precise control of power quality, harmonic content, and voltage levels [27].The fundamental relation between the AC voltage and the DC link voltage of a VSC can also be expressed as

$$V_{\text{ac}} = m\frac{V_{\text{dc}}}{2} \tag{12}$$

where m is the sinusoidal modulation index ($-1 \leq m \leq 1$) and V_{dc} is the input DC link voltage. This relation illustrates how the AC voltage and modulation directly determine the DC output and therefore highlights the bidirectional controllability of the VSC. By adjusting m, the converter not only regulates the AC-side voltage and power exchange but also maintains tight control of the DC link, ensuring stable operation when supplying electrolyzers.

In the context of electrolysis for hydrogen production, VSCs are particularly advantageous due to their superior power quality and control capabilities. Electrolysis systems benefit greatly from stable voltage and current control, which directly impacts the efficiency and longevity of the electrolyzers [41], [42]. The ability of VSCs to minimize harmonic distortion and precisely regulate output power ensures that the electrolyzer operates at optimal conditions. However, VSCs also have certain drawbacks, including higher initial costs, increased complexity in control systems, and their limitations in switching high currents, which can lead to increased stress on components and reduced efficiency in high-power operations.

Two distinct control strategies are conceivable for this type of converter: grid-following and grid-forming, both illustrated in Fig. 15. In grid-following control, a phase-locked loop (PLL) is used to track the grid frequency, ensuring that the converter's output current is synchronized with the grid. This method essentially makes the converter "follow" the grid, meaning its operation is related to an external grid [43], [44], [45], [46]. While grid-following control schemes enable precise active/reactive power regulation, they can become unstable in weak-grid conditions or during islanded operation, where low short-circuit ratio (SCR) levels may cause PLL loss of synchronization and degraded dynamic support [45], [46]. Conversely, grid-forming control allows the converter to establish its own voltage and frequency reference. Based on that, this control strategy is capable of operating in weak grid conditions,

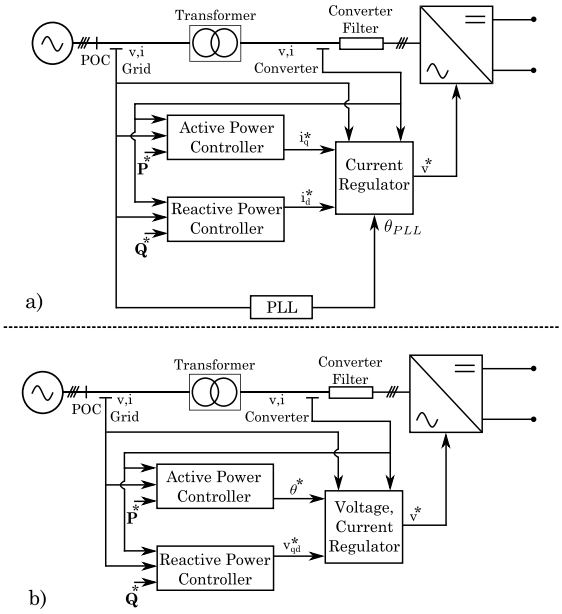

FIGURE 15. a) Grid-following b) Grid-forming.

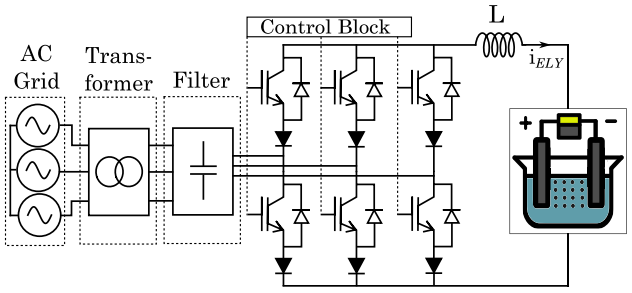

FIGURE 16. Current source converter.

islanded operation [47], [48], [49], [50], [51]. Grid-forming converters thereby offer black-start capability and robust microgrid performance, but they demand careful tuning of droop coefficients to maintain stability in meshed networks and may exhibit slower transient response when high virtual-inertia emulation is applied [48], [49]. In practice, grid-following architectures are best deployed on strong grids with well-defined voltage references, whereas grid-forming designs excel in weak-grid or islanded scenarios and when ancillary services are required.

Beyond supplying high-quality DC power to the electrolyzer, VSCs also enable a wide range of grid support functions that cannot be provided by diode- or thyristor-based rectifiers. Through advanced control strategies, VSCs can provide services such as fault ride-through (FRT), i.e., the ability to remain connected during voltage dips; voltage support, by exchanging reactive power to stabilize grid voltage; frequency support, by modulating power consumption to assist grid frequency stability; and black-start or islanded operation, possible when equipped with grid-forming control, allowing the converter to function without an external grid reference. These capabilities are essential in future grids with high penetration of renewable energy sources and represent one of the most critical future roles of large-scale electrolyzers, transforming them from passive loads into active grid-stabilizing assets. It should be noted, however, that the extent to which electrolyzers can provide these services is subject to plant-level constraints such as ramp-rate limitations, minimum load requirements, and auxiliary system dynamics, as discussed in [52].

B. CURRENT SOURCE CONVERTER

The circuit diagram of a current source converter (CSC) is shown in Fig. 16. As depicted, IGBT switches are in series with diodes (also possible with GTOs), which can lead to higher Joule losses at high currents [30].

A three-phase filter capacitor is generally required at the CSC's input, serving two primary purposes: (a) aiding in the commutation of switching devices; (b) filtering out line current harmonics. However, the use of a filter capacitor may introduce LC resonances, which can negatively impact the converter's input power factor. The size of the capacitor is determined by several factors, including switching frequency, LC resonance mode, total harmonic distortion (THD) requirements, and input power factor [53].

On the DC side, an inductor is required to smooth the DC current. This inductor, commonly referred to as a DC choke, helps in limiting current ripple and stabilizing the rectifier's output [54]. Additionally, CSCs inherently provide shortcircuit protection due to the high impedance of the inductor, which limits sudden current surges.

Despite the favorable results of this topology, which can be observed in [55], CSCs may not be the ideal option for electrolysis due to higher losses, complex filtering requirements, and lower power factor under varying loads [56], [57], [58]. Until better control strategies are developed, VSCs remain the preferred alternative for high-power electrolysis systems.

VI. TWO-STAGE CONVERTERS

Since high-power electrolyzers demand low voltage amplitudes (a few hundred volts) and extremely high current (in the kA range), a two-stage converter can mitigate the challenges of handling extremely high current by increasing the voltage at the rectifier, which reduces the current for the same power level and alleviates the stress on the switches [30]. Then, with the help of the buck converter, the DC voltage can be reduced to the required value for the electrolyzer. In reality, this combination increases the power factor due to smoother and less rippled voltage without resorting to costly low-harmonic passive filters [5]. Several topologies that might be particularly advantageous for electrolysis applications are described in this section.

A. BRIDGE RECTIFIER WITH A BUCK CONVERTER

According to Fig. 17, a six-pulse diode bridge rectifier may be coupled to a buck converter, offering high efficiency and effective control [59]. Its hierarchy of operation begins

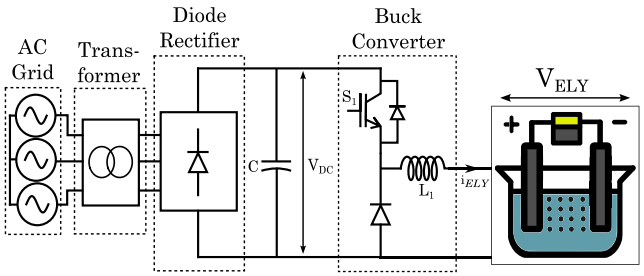

FIGURE 17. Bridge rectifier with a buck converter.

with the bridge rectifier, which produces a DC voltage that is comparatively acceptable and continues with the step-down buck converter, which controls the output voltage by controlling the current that flows through the switch S_1 and is highly dependent on the duty cycle value. By excluding the parasitic components, the buck converter's output voltage is stated as [27]

$$V_{\text{ELY}} = DV_{DC} \tag{13}$$

where D is the ratio of the conduction of the switch and the switching period, which is called the duty cycle, and it may vary between 0 and 1. The output current ripple can be also written as [27]

$$\Delta i_{\text{ELY}} = \frac{DV_{DC}(1-D)}{L_1 f_s}, \tag{14}$$

where L_1 is the inductor value in H and f_s is the switching frequency in Hz of the switch S_1. From (14) it is clear that switching frequency and inductor value play a critical role in reducing the current ripple, which is essential for electrolysis operation since it may alter the dynamic and efficiency of the electrolyzer and may also damage its aging [60]. The design challenge lies in balancing the higher cost and volume of larger inductors with the increased switching losses at higher frequencies, requiring an optimal trade-off [27]. The major downside of this topology is reliability because there is only one switch, which puts a lot of strain on the switch itself and causes the system to shut down in the event of a switch failure.

B. BRIDGE RECTIFIER WITH A THREE-PHASE INTERLEAVED BUCK CONVERTER

Three independent buck branches are taken into consideration in this architecture for the DC-DC converter, as shown in Fig. 18. A completely controllable switch, a diode, and an inductor constitute each branch. The switching excitation signal of each branch has a phase difference of 1/3 of a cycle, or a phase shift angle of 120°, and is driven by a switch signal of the same frequency [21]. Less current ripple, greater energy efficiency, and dependability make this system preferable to a single buck converter. The splitting of current among the three switches improves efficiency and enhances resilience, allowing the system to operate with the remaining switches in case of a failure. By taking into consideration that the voltage ripple equation is the same as a single branch buck

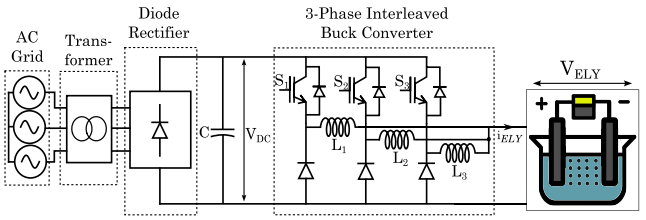

FIGURE 18. Bridge rectifier with three-phase interleaved buck converter.

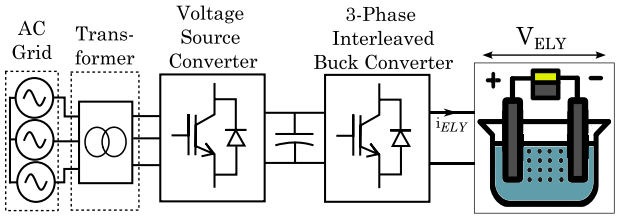

FIGURE 19. VSC with three-phase interleaved buck converter.

converter as stated in (14), the current ripple can be written as [5]

$$\Delta i_{\text{ELY}} = \begin{cases} \dfrac{V_{\text{ELY}} D(1-3D)}{L f_s}, & 0 < D < \dfrac{1}{3} \\ \dfrac{V_{\text{ELY}}(3D-1)(2-3D)}{3L f_s}, & \dfrac{1}{3} < D < \dfrac{2}{3} \\ \dfrac{V_{\text{ELY}}(3D-2)D}{L f_s}, & \dfrac{2}{3} < D < 1 \end{cases} \tag{15}$$

Equations above make it evident that by allocating 1/3 of the intended duty cycle to each branch, the current will be distributed according to that ratio, but in the event of a failure, such as one switch, the allotted duty cycle for the other switches would increase to 50% to make up for the share of the lost switch, which supports the robustness of this topology.

C. VSC AND BUCK CONVERTER

Thyristor-based and uncontrolled rectifiers are inadequate for grid support tasks such as fault ride-through, as now mandated by the new German grid code [61]. The recent regulation mandates that systems remain connected during fault conditions. As a result, VSCs provide a viable alternative to meet these grid code requirements. To deliver reduced current ripple to the electrolyzer and reduced current per branch to the DC-DC converter, a three-phase interleaved buck converter can be integrated into the DC link. This configuration enables the VSC to manage the required power effectively, as illustrated in Fig. 19.

The advantages of using a VSC include: a) controlling active and reactive power separately; b) eliminating the risk of commutation failures. This architecture is ideal for grid services, connecting to weak AC networks, and offering faster dynamic response due to higher switching frequencies [62].

The three-phase interleaved DC-DC buck converter is ideal for its advantages in voltage ratio, efficiency, current

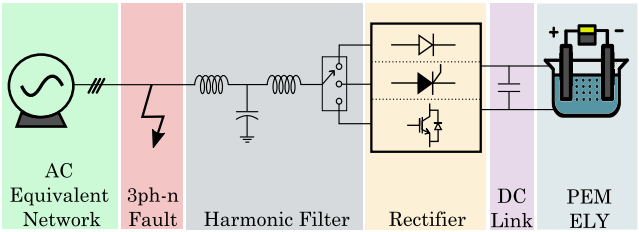

FIGURE 20. System description under the analysis.

ripples, and reliability [63], [64]. This topology is well-suited for high-power multi-source systems, including renewable energy and hydrogen technologies [65].

As electrolyzer capacities scale beyond a few megawatts, two-level and three-level VSCs face challenges in device stress and filtering requirements. Modular multilevel converters (MMCs) overcome these by assembling each phase leg from many series-connected submodules, so that no single semiconductor sees the full DC-link voltage. This architecture delivers near-sinusoidal waveforms with minimal filtering, intrinsic redundancy to tolerate submodule failures, and straightforward scalability to higher voltages and powers [66]. These features make MMCs especially attractive for next-generation, ultra-high-power hydrogen production systems.

It is worth mentioning that certain long-term effects, such as degradation, are not yet fully represented in established electrolyzer models. In addition, other dynamic features such as ramp-rate constraints and gas dynamics are generally not included, owing to the limited availability of validated experimental data. Nevertheless, recent experimental studies have shown that power quality, particularly current ripple, plays a critical role in electrolyzer durability [67], [68]. Ripple-induced overpotentials increase local heating and accelerate membrane and electrode wear, especially in PEM systems. This underscores the added value of advanced converters such as VSCs, two-stage converters, and MMCs in delivering smooth DC power that enhances both efficiency and lifetime.

VII. COMPARISON OF POWER CONVERTER TOPOLOGIES

To demonstrate the capabilities and impact of different rectification technologies on the grid, a simulation has been conducted to analyze their behavior under both normal and fault conditions. While various converter topologies were discussed in the review, the selection of diode bridge rectifier, Graetz thyristor rectifier, and VSC for this study was made based on two key criteria.

- The objective is to compare diode- and thyristor-based rectifiers with the VSCs in terms of power quality, fault response, and controllability.
- The bridge and Graetz rectifiers represent the whole family of uncontrolled and controlled rectifiers for the objective of this study. Although the two-stage converters are not considered, the focus remains on the dynamics of interactions with the grid.

TABLE 3. System parameters.

Parameter	Value
AC Grid	
Nominal power	1 MVA
Nominal voltage	200 V
Frequency	50 Hz
SCR	10
PEM ELY	
Nominal power	0.9 MW
Reversible voltage V_{rev}	350 V
Double layer phenomenon C_a	0.16 μF
Double layer phenomenon R_a	0.04 Ω
Ohmic losses R_{mem}	0.01 Ω
Diode rectifier (DR)	
Harmonic inductive filter L_{ac}	0.2 pu
Harmonic capacitive filter C_{ac}	0.1 pu
Thyristor rectifier (TR)	
Harmonic inductive filter L_{ac}	0.2 pu
Harmonic capacitive filter C_{ac}	0.1 pu
VSC	
Harmonic inductive filter L_{ac}	0.08 pu
Harmonic capacitive filter C_{ac}	0.05 pu
Switching frequency F_{sw}	15 KHz

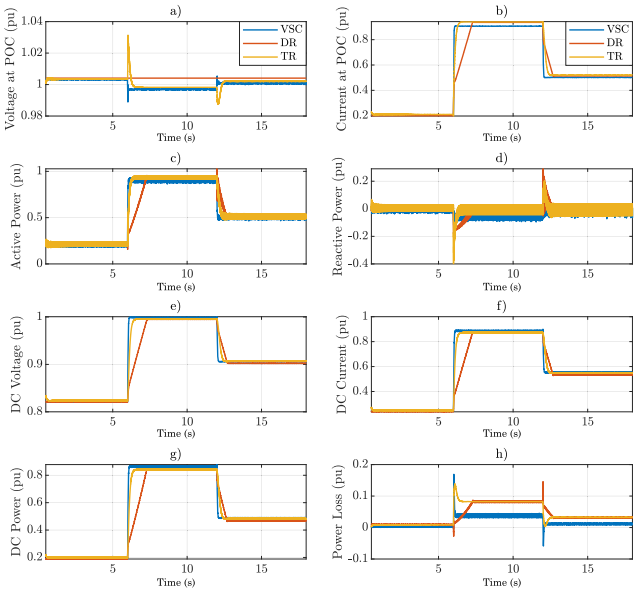

FIGURE 21. Normal operational results, power set points 0.2, 0.9, 0.5 pu at 0, 6, 12 seconds: a) Voltage at POC (pu), b) Current at POC (pu), c) Active power (pu), d) Reactive power (pu), e) DC voltage (pu), f) DC current (pu), g) DC power (pu), h) Power loss (pu).

The selected topologies are illustrated in Fig. 5, Fig. 11, and Fig. 14. The system under study is described in Fig. 20, and the parameters used in the simulations are provided in Table 3. It should be noted that the electrolyzer model used in this study is an equivalent model of the PEM electrolyzer, as described in Section II. As reported in [22], the dynamic model of the PEM electrolyzer achieves a maximum error of approximately 4% when reproducing real stack dynamics, compared to about 15% error for the static model. For this reason, the dynamic model was adopted in the present study to more accurately capture the relevant transient behavior.

TABLE 4. Overall comparison of rectifier technologies—key metrics for power quality, dynamic response, grid-support capabilities, and economic drivers (CAPEX, OPEX, maintenance) [30], [72], [73], [74], [75], [76], [77], [78], [79], [80], [81], [82].

Indices	Diode-Based Rectifier	Thyristor-Based Rectifier	DR+BUCK	VSC
Input Power Factor	Up to 0.96 at maximum load remains high across the entire load range	Can be adjusted to the desired value under full load, but drops dramatically at minimal load.	Up to 0.96 at maximum load remains high across the entire load range	Unity
Harmonic Distortion	High	Very high, especially at minimum load	High	Very Low
Dynamics	Very slow (few s)	Slow (10-30 ms)	Fast (<1 ms)	Fast (<1 ms)
Output Voltage Ripple	Big filters required to minimize the ripple	Big filters required to minimize the ripple	Small filters due to the chopper section	Smaller filter due to the medium frequency operation
Input Filter	Passive	Passive tuned filters	Passive	Inductive filter to minimize high-frequency components
Control Flexibility	None	Low	Low	Complex
Reliability	High	Relatively high	Medium	Medium
Weak Grid Compability	Limited	Limited	Limited	High
Voltage Regulation Capability	None	None	None	Advanced
Frequency Support Functionality	Limited	Limited	Limited	Advanced
Power Ratings	Low (<500 kW)	High-Ultra high (>1 MW)	Ultra high (>3 MW)	Medium-High (<2 MW)
CAPEX	~300 USD/kW	~400 USD/kW	~450 USD/kW	~600 USD/kW
OPEX	2% (CAPEX/yr)	2.5% (CAPEX/yr)	2.5% (CAPEX/yr)	3% (CAPEX/yr)
Maintenance Intervals	5 (yrs)	4 (yrs)	4 (yrs)	3 (yrs)

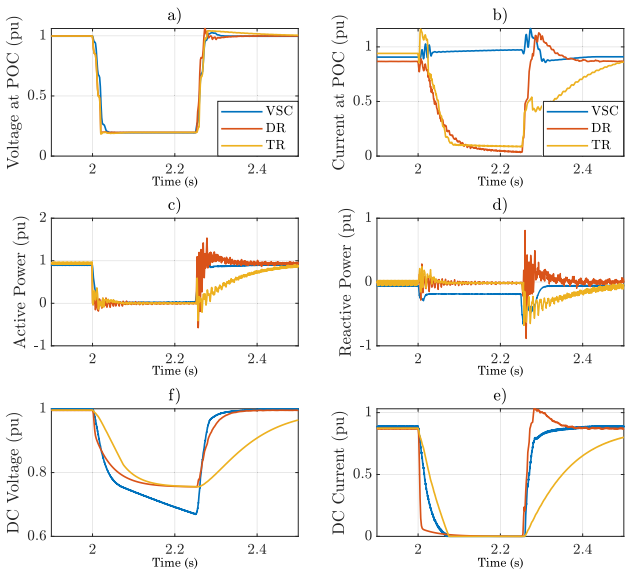

FIGURE 22. Fault analysis results, voltage dip 0.2 pu for 250ms: a) Voltage at POC (pu), b) Current at POC (pu), c) Active power (pu), d) Reactive power (pu), e) DC voltage (pu), f) DC current (pu).

The normal operational analysis results are illustrated in Fig. 21. The power set points for this analysis are 0.2, 0.9, and 0.5 per unit (pu) at 0, 6, and 12 seconds, respectively. Each topology employs a distinct control design. For instance, the VSC employs a grid-following control strategy, as detailed in Section VI. The thyristor rectifier utilizes a current controller, as described in Section IV. In the case of the diode rectifier, an auto-transformer is assumed to be connected at the Point of Connection (POC). The auto-transformer controls the rectifier's input voltage, thereby regulating the power injected to the electrolyzer. In terms of filter design, an LCL filter for the VSC was designed and implemented based on the methodology detailed in [69]. For the thyristor and diode rectifiers, a combination of series static and trap filters, along with controlled static inductors and capacitor banks, was considered to maintain the unity power factor at the point of connection.

As is clear, all topologies supply the electrolyzer with DC power as required. However, due to the high switching frequency of the VSC, it requires smaller DC link filters compared to the larger filters needed for diode and thyristor rectifiers to achieve the same power quality in terms of voltage and current ripple. Additionally, in terms of response time, VSC is the fastest (see Fig. 21 c), followed by the thyristor rectifier, and then the diode rectifier. The reason for this is that the VSC and thyristor-based rectifiers use faster switches and control compared to the tap changers of the auto-transformer used in the diode-based rectifier.

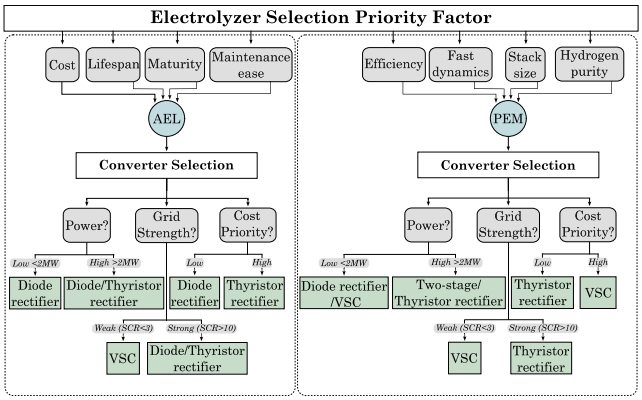

FIGURE 23. Simplified flowchart for selecting electrolyzer type and converter topology based on project priorities.

Furthermore, the VSC is faster than the thyristor rectifier due to the use of IGBTs. Another notable difference is the power losses; the VSC has lower power losses (See Fig. 21 h) due to requiring fewer harmonic filters compared to the thyristor and diode rectifiers.

The fault results in Fig. 22 demonstrate three stages: pre-fault, fault, and post-fault conditions. At 2 s, the voltage at POC drops to 0.2 pu, and the fault persists for 250 ms until it is cleared. Across the three technologies examined, when a fault occurs, active power to the PEM electrolyzer is reduced to zero. The difference lies in the response mechanism; for traditional rectifiers, such as diode-based and thyristor-based rectifiers, this is a natural response because of lower forward bias due to low AC voltage. However, in VSC, the control system is responsible for its action. Additionally, the VSC can be configured to maintain load supply during this period, but this would require an appropriately designed energy storage system [70].

The main difference to note is the capability of injecting reactive current during the fault for voltage support. Among these three technologies, only VSC can achieve it due to the implementation of a voltage droop controller. This is also shown in the current results at the POC, where the VSC increases its current to the injection of 1 pu reactive current into the grid (Fig. 22 b). In general, a comparison between the technologies mentioned above is gathered in Table 4.

Although this work is primarily simulation-based, obtaining detailed field measurements for large electrolyzers is difficult. As a representative example, the European Synergy Action TSO2020 project commissioned a 1 MW PEM electrolyzer at Veendam–Zuidwending (Groningen, Netherlands). An RSCAD/RTDS model of this unit was tuned and validated against on-site measurements, confirming the fast dynamic response and reactive-current injection capabilities predicted by this study [71].

Finally, to provide a clearer guideline for selecting between electrolyzer technologies and the associated converter topologies discussed in this study, a simplified decision flowchart is presented in Fig. 23.

VIII. CONCLUSION

This paper reviewed and analyzed various rectifier topologies for electrolysis applications, highlighting their benefits and drawbacks. Diode rectifiers, despite their reliability and robustness, suffer from a lack of control and significant voltage ripple. Thyristor-based rectifiers, commonly used in high-power applications due to their robust nature, contribute to high harmonic distortion, requiring large compensators to maintain power quality.

VSCs emerged as an attractive solution due to their fast response times and lower harmonic distortion. However, their switching limitations under high current conditions make them less suitable for very high-power applications. To address this, the study included coupling the VSC with a DC-DC buck converter to handle high currents effectively while also enabling grid services through the VSC.

Simulation of three main topologies provides a comparison of the electrolyzer operation, showing that VSCs offer better power quality with reduced voltage and current ripple compared to diode and thyristor rectifiers. Furthermore, VSCs demonstrated superior performance in fault conditions, providing fault ride-through capability and reactive current injection, highlighting their potential for future power networks where flexibility is essential.

In conclusion, while uncontrolled and thyristor-based rectifiers have their merits, VSCs offer significant advantages in terms of power quality, response time, and grid support, making them a promising solution for large-scale electrolysis.

This review has focused on two representative cases, active power variation and a balanced three-phase fault, which are sufficient to illustrate the fundamental dynamic differences among converter topologies for electrolyzer applications. As this article is primarily a review, a comprehensive simulation campaign covering all possible operating conditions was beyond the intended scope. Nevertheless, future research should extend the analysis to include unbalanced faults, voltage sags, and frequency excursions, as well as integrate degradation mechanisms and ramp-rate limits into electrolyzer models. Such studies will help validate and refine the insights presented here, ultimately contributing to a more complete framework for converter electrolyzer integration in large-scale hydrogen systems.

ACKNOWLEDGMENT

Views and opinions expressed are however those of the authors only and do not necessarily reflect those of the European Union or the European Health And Digital Executive Agency. Neither the European Union nor the granting authority can be held responsible for them.

REFERENCES

[1] (2020). *Making Mission Possible: Delivering a Net-Zero Economy*. [Online]. Available: https://www.energy-transitions.org/publications/making-mission-possible/

[2] International Energy Agency. *Hydrogen Supply-Analysis*. [Online]. Available: https://www.iea.org/reports/hydrogen-supply

[3] M. Petrova. (2020). *Green Hydrogen is Gaining Traction, but Still Has Massive Hurdles To Overcome*. [Online]. Available: https://www.cnbc.com/2020/12/04/green-hydrogen-is-gaining-traction-but-it-must-overcome-big-hurdles.html

[4] A. Ajanovic, M. Sayer, and R. Haas, "The economics and the environmental benignity of different colors of hydrogen," *Int. J. Hydrogen Energy*, vol. 47, no. 57, pp. 24136–24154, Jul. 2022. [Online]. Available: https://www.sciencedirect.com/science/article/pii/S0360319922007066

[5] B. Yodwong, D. Guilbert, M. Phattanasak, W. Kaewmanee, M. Hinaje, and G. Vitale, "AC–DC converters for electrolyzer applications: State of the art and future challenges," *Electronics*, vol. 9, no. 6, p. 912, May 2020.

[6] Y. Guo, G. Li, J. Zhou, and Y. Liu, "Comparison between hydrogen production by alkaline water electrolysis and hydrogen production by PEM electrolysis," *IOP Conf. Ser., Earth Environ. Sci.*, vol. 371, Dec. 2019, Art. no. 042022.

[7] *Hydrogen Production: Electrolysis*. Accessed: June. 23, 2024. [Online]. Available: https://www.energy.gov/eere/fuelcells/hydrogen-production-electrolysis:~:text=Electrolysis%20is%20the%20process%20of

[8] T. Letcher and T. M. Letcher, *Comprehensive Renewable Energy*. Amsterdam, The Netherlands: Elsevier, 2022.

[9] P. E. Miranda, *Science and Engineering of Hydrogen-Based Energy Technologies : Hydrogen Production and Practical Applications in Energy Generation*. Amsterdam, The Netherlands: Elsevier, 2018.

[10] C. Azzaro-Pantel, *Hydrogen Supply Chain: Design, Deployment and Operation*. New York, NY, USA: Academic, 2018.

[11] M. David, C. Ocampo-Martínez, and R. Sánchez-Peña, "Advances in alkaline water electrolyzers: A review," *J. Energy Storage*, vol. 23, pp. 392–403, Jun. 2019.

[12] R. Costa and P. Grimes, "Electrolysis as a source of hydrogen and oxygen," *Chem. Eng. Prog.*, vol. 63, no. 4, pp. 56–58, Apr. 1967.

[13] R. Phillips and C. W. Dunnill, "Zero gap alkaline electrolysis cell design for renewable energy storage as hydrogen gas," *RSC Adv.*, vol. 6, no. 102, pp. 100643–100651, 2016. [Online]. Available: https://pubs.rsc.org/en/content/articlelanding/2016/ra/c6ra22242k

[14] F. Gambou, D. Guilbert, M. Zasadzinski, and H. Rafaralahy, "A comprehensive survey of alkaline electrolyzer modeling: Electrical domain and specific electrolyte conductivity," *Energies*, vol. 15, no. 9, p. 3452, May 2022.

[15] Á. Hernández-Gómez, V. Ramirez, D. Guilbert, and B. Saldivar, "Cell voltage static-dynamic modeling of a PEM electrolyzer based on adaptive parameters: Development and experimental validation," *Renew. Energy*, vol. 163, pp. 1508–1522, Jan. 2021. [Online]. Available: https://www.sciencedirect.com/science/article/pii/S0960148120315317

[16] W. T. Grubb, "Batteries with solid ion exchange electrolytes," *J. Electrochemical Soc.*, vol. 106, no. 4, p. 275, 1959.

[17] W. T. Grubb, "Ionic migration in ion-exchange membranes," *J. Phys. Chem.*, vol. 63, no. 1, pp. 55–58, Jan. 1959.

[18] S. S. Kumar and V. Himabindu, "Hydrogen production by PEM water electrolysis—A review," *Mater. Sci. Energy Technol.*, vol. 2, pp. 442–454, Mar. 2019.

[19] C. Xiang, K. M. Papadantonakis, and N. S. Lewis, "Principles and implementations of electrolysis systems for water splitting," *Mater. Horizons*, vol. 3, no. 3, pp. 169–173, 2016.

[20] M. Schalenbach, M. Carmo, D. L. Fritz, J. Mergel, and D. Stolten, "Pressurized PEM water electrolysis: Efficiency and gas crossover," *Int. J. Hydrogen Energy*, vol. 38, no. 35, pp. 14921–14933, Nov. 2013.

[21] M. Carmo, D. L. Fritz, J. Mergel, and D. Stolten, "A comprehensive review on PEM water electrolysis," *Int. J. Hydrogen Energy*, vol. 38, pp. 4901–4934, Apr. 2013.

[22] D. Guilbert and G. Vitale, "Dynamic emulation of a PEM electrolyzer by time constant based exponential model," *Energies*, vol. 12, no. 4, p. 750, Feb. 2019.

[23] B. Yodwong, D. Guilbert, M. Phattanasak, W. Kaewmanee, M. Hinaje, and G. Vitale, "Proton exchange membrane electrolyzer modeling for power electronics control: A short review," *C*, vol. 6, no. 2, p. 29, May 2020.

[24] F. da Costa Lopes and E. H. Watanabe, "Experimental and theoretical development of a PEM electrolyzer model applied to energy storage systems," in *Proc. Brazilian Power Electron. Conf.*, Sep. 2009, pp. 775–782.

[25] A. Chandrasekar, D. Flynn, and E. Syron, "Operational challenges for low and high temperature electrolyzers exploiting curtailed wind energy for hydrogen production," *Int. J. Hydrogen Energy*, vol. 46, no. 57, pp. 28900–28911, Aug. 2021.

[26] J. Biela, D. Hassler, J. Schönberger, and J. W. Kolar, "Closed-loop sinusoidal input-current shaping of 12-pulse autotransformer rectifier unit with impressed output voltage," *IEEE Trans. Power Electron.*, vol. 26, no. 1, pp. 249–259, Jan. 2011.

[27] M. H. Rashid, *Power Electronics Handbook*. Amsterdam, The Netherlands: Elsevier, 2001.

[28] D. W. Hart, *Power Electronics*. New York, NY, USA: McGraw-Hill, 2010.

[29] R. Wu, F. Blaabjerg, H. Wang, and M. Liserre, "Overview of catastrophic failures of freewheeling diodes in power electronic circuits," *Microelectron. Rel.*, vol. 53, nos. 9–11, pp. 1788–1792, Sep. 2013. [Online]. Available: https://www.sciencedirect.com/science/article/pii/S0026271413003028

[30] J. Solanki, N. Fröhleke, J. Böcker, A. Averberg, and P. Wallmeier, "High-current variable-voltage rectifiers: State of the art topologies," *IET Power Electron.*, vol. 8, no. 6, pp. 1068–1080, Jun. 2015.

[31] J. Koponen, V. Ruuskanen, A. Kosonen, M. Niemelä, and J. Ahola, "Effect of converter topology on the specific energy consumption of alkaline water electrolyzers," *IEEE Trans. Power Electron.*, vol. 34, no. 7, pp. 6171–6182, Jul. 2019.

[32] F.-W. Speckmann, S. Bintz, and K. P. Birke, "Influence of rectifiers on the energy demand and gas quality of alkaline electrolysis systems in dynamic operation," *Appl. Energy*, vol. 250, pp. 855–863, Sep. 2019.

[33] G. W. Ndiwulu, E. V. Mayen, and E. De Jaeger, "Dynamic interactions of a high-current thyristor-rectifier interfaced PEM electrolyzer with the angular dynamics of synchronous machines," in *Proc. IEEE Int. Conf. Environ. Electr. Eng. IEEE Ind. Commercial Power Syst. Eur. (EEEIC / I&CPS Eur.)*, Jun. 2024, pp. 1–6.

[34] E. Kimbark, *Direct Current Transmission*. Hoboken, NJ, USA: Wiley, 1971. [Online]. Available: https://books.google.es/books?id=j-0OzQEACAAJ

[35] M. Cheah-Mane, J. Song, R. Ferrer-San-Jose, E. Prieto-Araujo, and O. Gomis-Bellmunt, "Analysis of hybrid LCC-VSC HVDC transmission system configurations," in *Proc. 15th IET Int. Conf. AC DC Power Transmiss. (ACDC)*, Feb. 2019, pp. 1–6.

[36] S. Mukhopadhyay, "A new concept for improving the performance of phase-controlled converters," *IEEE Trans. Ind. Appl.*, vol. IA-14, no. 6, pp. 594–603, Nov. 1978.

[37] T. Yuan, H. Li, J. Wang, and D. Jia, "Research on the influence of ripple voltage on the performance of a proton exchange membrane electrolyzer," *Energies*, vol. 16, no. 19, p. 6912, Sep. 2023. [Online]. Available: https://www.mdpi.com/1996-1073/16/19/6912

[38] M. Keddar, Z. Zhang, C. Periasamy, and M. L. Doumbia, "Comparative analysis of thyristor-based and transistor-based rectifiers for PEM water electrolysis," in *Proc. 12th Int. Renew. Energy Congr. (IREC)*, Oct. 2021, pp. 1–5.

[39] J. Solanki, N. Fröhleke, and J. Böcker, "Implementation of hybrid filter for 12-pulse thyristor rectifier supplying high-current variable-voltage DC load," *IEEE Trans. Ind. Electron.*, vol. 62, no. 8, pp. 4691–4701, Aug. 2015.

[40] A. Yazdani and R. Iravani, *Voltage-Sourced Converters in Power Systems: Modeling, Control, and Applications*. Hoboken, NJ, USA: Wiley, 2010.

[41] J. Lei, H. Ma, G. Qin, Z. Guo, P. Xia, and C. Hao, "A comprehensive review on the power supply system of hydrogen production electrolyzers for future integrated energy systems," *Energies*, vol. 17, no. 4, p. 935, Feb. 2024. [Online]. Available: https://www.mdpi.com/1996-1073/17/4/935

[42] M. Arunachalam and D. S. Han, "Efficient solar-powered PEM electrolysis for sustainable hydrogen production: An integrated approach," *Emergent Mater.*, vol. 7, no. 4, pp. 1401–1415, Aug. 2024, doi: 10.1007/s42247-024-00697-y.

[43] A. Egea-Àlvarez, A. Junyent-Ferré, and O. Gomis-Bellmunt, "Active and reactive power control of grid connected distributed generation systems," in *Modeling and Control of Sustainable Power Systems* (Green Energy and Technology). Springer, Nov. 2011, pp. 47–81.

[44] X. Gao, D. Zhou, A. Anvari-Moghaddam, and F. Blaabjerg, "Grid-following and grid-forming control in power electronic based power systems: A comparative study," in *Proc. 47th Annu. Conf. IEEE Ind. Electron. Soc.*, Oct. 2021, pp. 1–6.

[45] B. Wen, D. Boroyevich, R. Burgos, P. Mattavelli, and Z. Shen, "Analysis of phase-locked loop low-frequency stability in three-phase grid-connected power converters considering impedance interactions," *IEEE Trans. Power Electron.*, vol. 31, no. 1, pp. 675–687, Jan. 2016.
[46] W. Du, F. K. Tuffner, K. P. Schneider, R. H. Lasseter, J. Xie, Z. Chen, and B. Bhattarai, "Modeling of grid-forming and grid-following inverters for dynamic simulation of large-scale distribution systems," *IEEE Trans. Power Del.*, vol. 36, no. 4, pp. 2035–2045, Aug. 2021.
[47] B. Barac, M. Krpan, T. Capuder, and I. Kuzle, "Modeling and initialization of a virtual synchronous machine for power system fundamental frequency simulations," *IEEE Access*, vol. 9, pp. 160116–160134, 2021.
[48] R. Rosso, X. Wang, M. Liserre, X. Lu, and S. Engelken, "Grid-forming converters: Control approaches, grid-synchronization, and future trends—A review," *IEEE Open J. Ind. Appl.*, vol. 2, pp. 93–109, 2021.
[49] Y. Li, Y. Gu, and T. C. Green, "Revisiting grid-forming and grid-following inverters: A duality theory," *IEEE Trans. Power Syst.*, vol. 37, no. 6, pp. 4541–4554, Nov. 2022.
[50] A. Zecchino, F. Gerini, Y. Zuo, R. Cherkaoui, M. Paolone, and E. Vagnoni, "Local effects of grid-forming converters providing frequency regulation to bulk power grids," in *Proc. IEEE PES Innov. Smart Grid Technol. - Asia (ISGT Asia)*, Dec. 2021, pp. 1–5.
[51] M. Tofighi–Milani, S. Fattaheian–Dehkordi, and M. Lehtonen, "Dynamic response analysis of alkaline and PEM electrolyzers in low-inertia power systems: A comparative study," in *Proc. IEEE Int. Conf. Environ. Electr. Eng. IEEE Ind. Commercial Power Syst. Eur. (EEEIC / I&CPS Eur.)*, Jun. 2024, pp. 01–06.
[52] N. Taranin, M. G. Dozein, O. Saborío-Romano, and N. A. Cutululis, "On the ramp-rate limitation of electrolysis plants: Modeling fundamentals and system-level impact analysis," *IEEE Trans. Sustain. Energy*, early access, Sep. 18, 2025, doi: 10.1109/TSTE.2025.3611711.
[53] B. Wu and M. Narimani, *High-power Converters and AC Drives*. Piscataway, NJ, USA: IEEE Press, 2017.
[54] B. Wu, S. Rizzo, N. Zargari, and Y. Xiao, "An integrated DC link choke for elimination of motor common-mode voltage in medium voltage drives," in *Proc. Conf. Rec. IEEE Ind. Appl. Conf., 36th IAS Annu. Meeting*, Dallas, TX, USA, Oct. 2001, pp. 2022–2027.
[55] J. Sau-Bassols, E. Prieto-Araujo, S. Galceran-Arellano, and O. Gomis-Bellmunt, "Operation and control of a current source converter series tapping of an LCC-HVDC link for integration of offshore wind power plants," *Electr. Power Syst. Res.*, vol. 141, pp. 510–521, Dec. 2016.
[56] B. Riegler and A. Muetze, "Passive component optimization for current-source-inverters," *IEEE Trans. Ind. Appl.*, vol. 59, no. 5, pp. 6113–6124, Sep. 2023.
[57] Y. Suh, J. Steinke, and P. Steimer, "A study on efficiency of voltage source and current source converter systems for large motor drives," in *Proc. 37th IEEE Power Electron. Specialists Conf.*, Jun. 2006, pp. 1–7.
[58] G. Ertasgin and D. M. Whaley, "Analysis and optimization of output low-pass filter for current-source single-phase grid-connected PV inverters," *Appl. Sci.*, vol. 14, no. 22, p. 10131, Nov. 2024. [Online]. Available: https://www.mdpi.com/2076-3417/14/22/10131
[59] M. Comanescu, A. Keyhani, and M. Dai, "Design and analysis of 42-v permanent-magnet generator for automotive applications," *IEEE Trans. Energy Convers.*, vol. 18, no. 1, pp. 107–112, Mar. 2003.
[60] H. P. C. Buitendach, R. Gouws, C. A. Martinson, C. Minnaar, and D. Bessarabov, "Effect of a ripple current on the efficiency of a PEM electrolyser," *Results Eng.*, vol. 10, Jun. 2021, Art. no. 100216.
[61] (2024). *Technische Anforderungen Für Den Anschluss Von Elektrolyseanlagen*. [Online]. Available: https://www.netztransparenz.de/en/About-us/Studies-and-position-papers/Requirements-for-the-connection-of-electrolyser-facilities
[62] K. Mohamed, Z. Ahmed, H. Samir, F. M. Karim, and A. Rabie. *Performance Analysis of a Voltage Source Converter VSC) Based HVDC Transmission System Under Faulted Conditions*. [Online]. Available: https://www.semanticscholar.org
[63] M. Ilic, B. Hesterman, and D. Maksimovic, "Interleaved zero current transition three-level buck converter," in *Proc. 21st Annu. IEEE Appl. Power Electron. Conf. Expo.*, Dallas, TX, USA, Mar. 2006, pp. 72–78.
[64] M. Ilic and D. Maksimovic, "Interleaved zero-current-transition buck converter," *IEEE Trans. Ind. Appl.*, vol. 43, no. 6, pp. 1619–1627, Jun. 2007.
[65] B. Yodwong, D. Guilbert, W. Kaewmanee, and M. Phattanasak, "Energy efficiency based control strategy of a three-level interleaved DC–DC buck converter supplying a proton exchange membrane electrolyzer," *Electronics*, vol. 8, no. 9, p. 933, Aug. 2019.
[66] Y. Li, Z. Wang, and J. Smith, "Modular multilevel converters for ultra-high-power electrolysis," *Energies*, vol. 17, no. 9, p. 2188, 2024.
[67] F. Parache, H. Schneider, C. Turpin, N. Richet, O. Debellemanière, É. Bru, A. T. Thieu, C. Bertail, and C. Marot, "Impact of power converter current ripple on the degradation of PEM electrolyzer performances," *Membranes*, vol. 12, no. 2, p. 109, Jan. 2022.
[68] G. Papakonstantinou, G. Algara-Siller, D. Teschner, T. Vidaković-Koch, R. Schlögl, and K. Sundmacher, "Degradation study of a proton exchange membrane water electrolyzer under dynamic operation conditions," *Appl. Energy*, vol. 280, Dec. 2020, Art. no. 115911.
[69] A. Reznik, M. G. Simões, A. Al-Durra, and S. M. Muyeen, "*LCL* filter design and performance analysis for grid-interconnected systems," *IEEE Trans. Ind. Appl.*, vol. 50, no. 2, pp. 1225–1232, Mar. 2014.
[70] P. Saha, W. Zhao, D.-I. Stroe, F. Iov, and S. Munk-Nielsen, "Enabling LVRT compliance of electrolyzer systems using energy storage technologies," *Batteries*, vol. 9, no. 11, p. 527, Oct. 2023. [Online]. Available: https://www.mdpi.com/2313-0105/9/11/527
[71] J. Rueda Torres, N. V. Kumar, E. Rakhshani, Z. Ahmad, E. Adabi, P. Palensky, and M. van der Meijden, "Dynamic frequency support for low inertia power systems by renewable energy hubs with fast active power regulation," *Electronics*, vol. 10, no. 14, p. 1651, Jul. 2021. [Online]. Available: https://www.mdpi.com/2079-9292/10/14/1651
[72] A. Siebert, A. Troedson, and S. Ebner, "AC to DC power conversion now and in the future," *IEEE Trans. Ind. Appl.*, vol. 38, no. 4, pp. 934–940, Jul. 2002.
[73] A. Agalgaonkar, K. Muttaqi, and S. Perera. *Response Analysis of Saturable Reactors and Tap Changer in an Aluminium Smelting Plant*. Accessed: Jan. 30, 2025. [Online]. Available: https://ro.uow.edu.au/cgi/viewcontent.cgi?article=8403context=engpapers
[74] P. Buddingh and J. R. St. Mars, "New life for old thyristor power rectifiers using contemporary digital control," *IEEE Trans. Ind. Appl.*, vol. 36, no. 5, pp. 1449–1454, May 2000.
[75] P. S. Maniscalco, V. Scaini, and W. E. Veerkamp, "Specifying DC chopper systems for electrochemical applications," *IEEE Trans. Ind. Appl.*, vol. 37, no. 3, pp. 941–948, May/Jun. 2001, doi: 10.1109/28.924779.
[76] J. Beak, P. Buddingh, and V. Scaini, "Reusing and rerating older rectifiers with new DC/DC choppers," *IEEE Trans. Ind. Appl.*, vol. 37, no. 4, pp. 1160–1166, Jul. 2001.
[77] A. K. Abdelsalam, M. I. Masoud, S. J. Finney, and B. W. Williams, "Medium-voltage pulse width modulated current source rectifiers using different semiconductors: Loss and size comparison," *IET Power Electron.*, vol. 3, no. 2, pp. 243–258, Mar. 2010.
[78] (2024). *DC Power Supply for Electrolyzers–Safe and Cost-Efficient Green Hydrogen Generation*. [Online]. Available: https://new.abb.com/drives
[79] AEG Power Solutions. (2023). *THYROBOXdc 3–Industrial DC Power Supply System for Green Hydrogen Production*. [Online]. Available: https://www.aegps.com
[80] Siemens. (2024). *SINAMICS PCS—The Power Conversion System for Industrial and Public Power Grids*. [Online]. Available: https://www.siemens.com/sinamics-pcs
[81] FRIEM. (2024). *Converters for Green Hydrogen Production*. [Online]. Available: https://www.friem.com
[82] Ingeteam Power Technology. (2024). *INGECON H2 C-Lyzer - Electrolyzer Converter Based on IGBT Technology*. [Online]. Available: https://www.ingeteam.com

MOHAMMADHOSSEIN TAVANAEE (Graduate Student Member, IEEE) received the M.S. degree in energy engineering from the Universitat Politècnica de Catalunya (UPC), in 2023, where he is currently pursuing the Ph.D. degree in electrical engineering. In 2023, he joined the CITCEA-UPC Research Group. His research interests include renewable energies, hydrogen systems, power system stability, and power electronics-dominated power systems.

JAUME GIRONA-BADIA (Member, IEEE) received the degree in industrial engineering from the School of Industrial Engineering of Barcelona (ETSEIB), Universitat Politècnica de Catalunya (UPC), Barcelona, Spain, in 2020. He is currently pursuing the Ph.D. degree with CITCEA-UPC. Since 2018, he has been with the CITCEA-UPC Research Group. His research interests include the fields linked with power electronics and renewable energy integration in power systems.

MARC CHEAH-MAÑE (Senior Member, IEEE) received the degree in industrial engineering from the School of Industrial Engineering of Barcelona (ETSEIB), Universitat Politècnica de Catalunya (UPC), Barcelona, Spain, in 2013, and the Ph.D. degree in electrical engineering from Cardiff University, Cardiff, U.K., in 2017. From 2017 to 2020, he was a Research Associate with CITCEA-UPC, Barcelona. From 2020 to 2024, he was a Lecturer under the Serra Húnter Program at the Electrical Engineering Department, UPC, and has been an Associate Professor, since 2024. Since 2022, he has been a Co-Founder of eRoots Analytics, a spin-off company of CITCEA-UPC. His research interests include power systems with power electronics, high-voltage direct current systems, ac/dc grids, and grid integration of wind and photovoltaic generation.

ORIOL GOMIS-BELLMUNT (Fellow, IEEE) received the degree in industrial engineering from the School of Industrial Engineering of Barcelona (ETSEIB), Universitat Politècnica de Catalunya (UPC), Barcelona, Spain, in 2001, and the Ph.D. degree in electrical engineering from UPC, in 2007. In 1999, he joined Engitrol S.L., where he was a Project Engineer in the automation and control industry. Since 2004, he has been with the Electrical Engineering Department, UPC, where he is a Professor and participates in the CITCEA-UPC Research Group. Since 2020, he has been an ICREA Academia Researcher. In 2022, he co-founded the start-up eRoots Analytics, focused on the analysis of modern power systems. His research interests include the fields linked with power electronics, power systems, and renewable energy integration in power systems.

EDUARDO PRIETO-ARAUJO (Senior Member, IEEE) received the degree in industrial engineering from the School of Industrial Engineering of Barcelona (ETSEIB), Universitat Politècnica de Catalunya (UPC), Barcelona, Spain, in 2011, and the Ph.D. degree in electrical engineering from UPC, in 2016. In 2010, he joined the CITCEA-UPC Research Group. He is currently a Serra Húnter Associate Professor with the Electrical Engineering Department, UPC. In 2021, he was a Visiting Professor with the Automatic Control Laboratory, ETH Zürich. In 2022, he co-founded eRoots, a spin-off company of CITCEA-UPC, focused on the analysis of modern power systems. His research interests include renewable generation systems, control of power converters for HVdc applications, interaction analysis between converters, and power electronics-dominated power systems.